Structure and dimerization of the catalytic domain of the protein phosphatase Cdc14p, a key regulator of mitotic exit in *Saccharomyces cerevisiae*

Junya Kobayashi [1] **and Yoshiyuki Matsuura** [1,2,*]

[1]*Division of Biological Science, and* [2]*Structural Biology Research Center, Graduate School of Science, Nagoya University, Japan*.

* Correspondence to: Yoshiyuki Matsuura, Division of Biological Science, Graduate School of Science, Nagoya University, Furo-cho, Chikusa-ku, Nagoya 464-8602, Japan.
E-mail: matsuura.yoshiyuki@d.mbox.nagoya-u.ac.jp

Running title: Structure and dimerization of budding yeast Cdc14p

Keywords: cell cycle; mitotic exit; protein phosphatase; Cdc14; dimerization

Supplementary Material:

Supporting Information (Figures S1 and S2) is supplied as a PDF file.

Filename: kobayashi2017ProtSci_suppl_submit.pdf

Abstract

In the budding yeast *Saccharomyces cerevisiae*, the protein phosphatase Cdc14p orchestrates various events essential for mitotic exit. We have determined the X-ray crystal structures at 1.85 Å resolution of the catalytic domain of Cdc14p in both the apo state, and as a complex with S160-phosphorylated Swi6p peptide. Each asymmetric unit contains two Cdc14p chains arranged in an intimately associated homodimer, consistent with its oligomeric state in solution. The dimerization interface is located on the backside of the substrate-binding cleft. Structure-based mutational analyses indicate that the dimerization of Cdc14p is required for normal growth of yeast cells.

Introduction

In eukaryotes, the regulation of mitotic exit involves inactivation of mitotic cyclin-dependent kinases (CDKs) and activation of counteracting protein phosphatases.[1] In the budding yeast *Saccharomyces cerevisiae*, the protein phosphatase Cdc14p is an antagonist of CDKs and is a key regulator of late mitotic events such as chromosome segregation, spindle disassembly, and cytokinesis.[2] The activity of Cdc14p is regulated through nucleolar sequestration.[3,4] Cdc14p is kept inactive from G1 to metaphase by its inhibitor Net1p (also known as Cfi1p), which sequesters Cdc14p in the nucleolus. During anaphase, Cdc14p is released from Net1p by at least two signaling networks (FEAR and MEN), and spreads throughout the cell where it antagonizes mitotic CDK activity and so returns the cell to G1. Cdc14p is also required for accurate segregation of ribosomal DNA (rDNA) and telomeres,[5,6] and inhibition of transcription of yeast ribosomal genes during anaphase.[7]

The budding yeast *CDC14* gene is essential for viability.[8] The budding yeast Cdc14p is composed of two domains. The N-terminal catalytic domain (residues 1-374) is necessary and sufficient for complementation of the *cdc14* null mutation.[9] The C-terminal domain (residues 375-551) is rich in asparagine and serine residues and is not required for the critical cell cycle function of Cdc14p.[9]

Cdc14 homologs have been identified in a wide range of organisms from yeast to humans.[10] Previously, crystal structure of the catalytic domain of human Cdc14B, one of the three Cdc14 homologs in humans, was determined, and revealed the molecular mechanism of the dephosphorylation reaction catalyzed by Cdc14 and provided structural evidence that Cdc14 selectively targets CDK phosphorylation sites (pS-P-x-K/R, where “pS” stands for phosphoserine, and “x” can be any amino acid).[11]

Because the Cdc14 residues at the catalytic site are highly conserved,[11] the catalytic mechanism is likely conserved from yeast to humans. However, there does not seem to be a conserved function of this phosphatase family throughout evolution,[10] and mitotic exit in animal cells seem to rely on phosphatases of the PP1 and PP2A families, despite the presence of Cdc14 homologs.[1]

In this study, we report the crystal structures of the catalytic domain of the budding yeast Cdc14p that formed an intimately associated homodimer in the asymmetric unit of the crystal. Structure-based mutational analyses provided a new biological insight that dimerization is important for the function of Cdc14p.

Results and Discussion

Structure determination

We obtained crystals of wild-type apo Cdc14p (residues 1-374) that belonged to the space group $P2_12_12_1$ and had unit cell parameters of a = 82.85 Å, b = 95.13 Å, c = 137.76 Å. The crystals contained two Cdc14p molecules per asymmetric unit, with a solvent content of 57%. The structure was determined at 1.85 Å resolution by molecular replacement. The final model of wild-type apo Cdc14p was refined to free and working R-factor values of 20.3% and 17.8%, respectively (Table I). A representative portion of the final $2F_o–F_c$ map is shown in Supporting Information Figure S1. Although V321 was a Ramachandran outlier, the electron density unambiguously showed the location of its carbonyl oxygen (Supporting Information Figure S1).

We next obtained crystals of apo C283S mutant of Cdc14p (residues 1-374) that is catalytically inactive but is capable of binding phosphorylated substrates.[9] The apo crystals of the C283S mutant were isomorphous to the wild-type apo crystals. To determine the structure of Cdc14p (C283S) bound to a phosphorylated substrate, we used a phosphopeptide (155-HRELG-pS-PLKK-164) derived from Swi6p, which is one of the physiological substrates of Cdc14p.[12] Swi6p is a transcription factor that is involved in cell-cycle-dependent transcription. The major cell cycle kinase Cdc28p and the S-phase cyclin Clb6p specifically phosphorylate Swi6p at S160 and direct nuclear export of Swi6p, whereas Cdc14p dephosphorylates pS160 and stimulates nuclear import of Swi6p.[12] After soaking the apo crystals of Cdc14p (C283S) with the S160-phosphorylated Swi6p peptide, we obtained a data set to 1.85 Å resolution and determined the structure by molecular replacement. Residues 157-164 of Swi6p bound to the catalytic site of Cdc14p chain A were identified unambiguously in the electron

density map [Fig. 1(A)], whereas the density map showed that a sulfate ion, instead of the phophopeptide, was bound to the catalytic site of Cdc14p chain B, probably because crystal packing hindered access of the phosphopeptide to this site of chain B. The final model of the phosphopeptide complex was refined to free and working *R*-factor values of 21.7% and 19.1%, respectively (Table I). The description of the Cdc14p structure below is based on the crystal structure of the phosphopeptide complex, but the conformation of the apo Cdc14p was essentially identical to that of Cdc14p in the phosphopeptide complex.

Overall structure of Cdc14p protomer

The two Cdc14p molecules in the asymmetric unit had essentially identical structure, with a root mean square deviation (r.m.s.d.) of Cα atoms of 0.285 Å. Similar to human Cdc14B [Fig. 1(B)], the catalytic domain of budding yeast Cdc14p is mainly composed of two similar domains [the N-terminal A-domain (residues 1-163) and the C-terminal B-domain (residues 171-342)], each with a dual-specificity protein phosphatase (DSP)-like fold, arranged in tandem [Fig. 1(C)]. The A-domain has four α-helices (α1A, α2A, α3A, and α4A) packed on one side of a β-sheet composed of four β-strands (β1A, β2A, β3A, and β4A) [secondary structure assignment, based on the method of Kabsch and Sander,[13] is depicted in Fig. 1(D)]. The B-domain has a β-sheet composed of five β-strands (β1B, β2B, β3B, β4B, and β5B) surrounded by α-helices with two (α1B and α2B) on one side and four (α3B, α4B, α5B, and α6B) on the opposite side. In the B-domain, the WPD loop (residues 249-258) connecting β4B with α3B bears the general acid/base D253 residue.[14] Also in the B-domain, the loop connecting β5B with α4B contains the active site sequence C-X_5-R (283-CKAGLGR-289), which is a hallmark for the protein tyrosine phosphatase (PTP) superfamily.[15] The A- and B-domains are connected by a linker helix, and the B-domain is followed by a

C-terminal extension that has two short β-strands (β1C and β2C) and a α-helix (α1C) [Fig. 1(C)].

Recognition of S160-phosphorylated Swi6p peptide by Cdc14p

The Swi6p phosphopeptide binds along the cleft formed at the interface of the A- and B-domains of Cdc14p [Fig. 1(C)] and buries 591 Å^2 of interfacial surface area. Swi6p forms an extensive network of interactions with Cdc14p residues at the catalytic site [Fig. 1(E)]. The phosphate group of the pS160^{Swi6p} side chain forms extensive hydrogen bonds with main chain amide groups of Cdc14p residues K284, A285, L287, G288, and R289, and also forms bidentate salt bridges with the guanidinium side-chain group of R289^{Cdc14p}. The aliphatic ring of the side chain of P161^{Swi6p} at the +1 position of the phosphorylation site (the P+1 position) fits into a nonpolar pocket formed by Cdc14p residues F47, A130, Y132, L287, and V322. The interactions between the Cdc14p catalytic site and the phosphoserine and the proline at the P+1 position of the substrate are quite similar to the interactions observed previously in the crystal structure of human Cdc14B bound to a phosphopeptide (A-pS-PRRR).[11] In addition, the structure of the budding yeast Cdc14p bound to the S160-phosphorylated Swi6p peptide also shows that the basic side chain of K163^{Swi6p} at the P+3 position binds to the acidic residues of Cdc14p (E171 and D177) that cluster at the entrance of the substrate-binding cleft. The aliphatic portion of the K163^{Swi6p} side chain is sandwiched between the nonpolar side chains of Cdc14p residues F47 and V173. These interactions are supplemented with hydrogen bonds between the main chain amide groups of Swi6p and the side chains of Cdc14p residues (Y132 and D253).

Dimerization of Cdc14p and its functional significance

The catalytic domain of Cdc14p forms an intimately associated homodimer in the asymmetric unit of the crystal [Fig. 2(A)]. Notably, the dimerization interface is quite extensive and buries 1668 $Å^2$ of the surface area of each chain, which is unusually large for normal crystal packing interfaces.[16] This is consistent with a previous biochemical study that suggested that the catalytic domain of Cdc14p most likely forms a homodimer *in vitro*.[9] The dimerization interface is located on the backside of the substrate-binding cleft [Fig. 2(A)]. The dimer interface residues (41 residues in each chain) are highlighted in stick representation in Figures 2(A) and 2(B). In this symmetrical homodimer, the A-domain of chain A mainly interacts with the A-domain of chain B, and the B-domain of chain A mainly interacts with the B-domain of chain B. The long loop (residues 118-140) connecting α3A with α4A and adjacent three α-helices (α2A, α3A, and α4A) are involved in the packing between the A-domains in the dimer. The long α-helix α6B and the adjacent short loop (residues 303-305) connecting α4B with α5B are involved in the packing between the B-domains in the dimer. These interactions are supplemented with interactions between α4A in the A-domain of one chain and α6B in the B-domain of the second chain in the dimer. This mode of dimerization was not observed previously in the crystal structure of human Cdc14B,[11] whose oligomeric state in solution and in living cells remains uncharacterized. The surface conservation profile of Cdc14 as analyzed by the ConSurf web server[17] is shown in Supporting Information Figure S2. Except for the highly conserved catalytic-site residues of Cdc14, the surface residues of Cdc14 are rather poorly conserved, indicating that the way Cdc14p chains form a dimer as observed in the crystal structures of Cdc14p may be specific to the budding yeast Cdc14p.

To verify that the dimer observed in the asymmetric unit of the Cdc14p crystals corresponds to Cdc14p dimer in solution, we engineered Cdc14p mutants in which the dimer interface observed in the crystal structures is specifically disrupted. We

made two mutants: P123E and Y146K/Y330K. Among the dimer interface residues, P123 is located at the "periphery" of the dimer interface, and the aliphatic ring of P123 of chain A packs against that of P123 of chain B [Fig. 2(A)]. Thus, the substitution of P123 with glutamic acid would disrupt a hydrophobic interaction at the dimer interface. Y146 and Y330 are located close to the "core" of the dimer interface [Fig. 2(A)]. The phenolic side chain of Y146 of chain B contacts that of Y330 of chain A, and also forms a hydrogen bond with H327 of chain A [Fig. 2(A)]. Y330 of chain A also forms a hydrogen bond with E308 of chain B [Fig. 2(A)]. Because this is a symmetrical homodimer, Y146 and E308 of chain A interact with Y330 and H327 of chain B in the same manner. Therefore, the double mutations Y146K/Y330K would effectively disrupt the intermolecular interactions at the dimer interface at two sites. We compared the oligomeric state of the Cdc14p mutants in solution with that of wild-type Cdc14p, using analytical gel filtration chromatography on a Superdex200 column. In gel filtration, His_6-Cdc14p (residues 1-374, wild-type) eluted as a single peak, and both P123E mutant and Y146K/Y330K mutant eluted later as a single peak [Fig. 2(C)]. Calibration of the Superdex200 column with molecular mass standards gave an apparent molecular mass of 76 kDa for wild-type and 33 kDa for the mutants [Fig. 2(D)], suggesting that the wild-type catalytic domain of Cdc14p forms a stable dimer but the mutants are unable to form a dimer under the condition tested *in vitro*.

We also analyzed the effects of mutations on the *in vivo* function of full-length Cdc14p. A haploid *cdc14Δ* strain containing an extrachromosomal wild-type copy of *CDC14* in a *CEN URA3* plasmid was transformed with *CEN LEU2* plasmids containing wild-type or mutant alleles of *CDC14* and selected on 5-fluoroorotic acid (5-FOA) media for the loss of *CEN URA3* [Fig. 2(E)]. As expected, wild-type *CDC14* complemented *cdc14Δ* lethality as opposed to vector alone [Fig. 2(E)]. Although the P123 mutation hardly affected yeast cell growth at 30 °C, it severely impaired growth at

37 °C [Fig. 2(F)]. The double mutant Y146K/Y330K exhibited more drastic phenotype. The mutations Y146K/Y330K severely impaired yeast cell growth both at 30 °C and 37 °C [Fig. 2(E)]. These data provide evidence that the dimer interface residues are important for Cdc14p function *in vivo*.

Conclusions

In summary, we have established the structures of the catalytic domain of budding yeast Cdc14p, the founding member of the Cdc14 family of dual-specificity phosphatases, in both the apo state (wild type) and a phophopeptide substrate-bound state (with a C to S substitution at the catalytic site). The structures defined the dimerization interface of Cdc14p on the backside of the catalytic site. Importantly, amino acid substitution(s) at the dimer interface of Cdc14p not only inhibited dimer formation in solution but also impaired yeast cell growth. These observations have the potential to open up new lines of inquiry into the functional role of the quaternary structure of Cdc14p.

Materials and Methods

Expression and purification of Cdc14p

N-terminally His_6-tagged Cdc14p (*S. cerevisiae*, residues 1-374; TEV site was inserted between the His_6-tag and Cdc14p) was expressed from pRSFDuet-1 (Novagen) in the *E. coli* host strain BL21-CodonPlus(DE3)RIL (Stratagene) at 25 °C in LB medium. His_6-Cdc14p (residues 1-374) was initially purified by Ni-NTA (Qiagen) chromatography with buffer A [30 mM Tris-HCl (pH 7.5), 0.5 M NaCl, 10 mM imidazole, 7 mM 2-mercaptoethanol, 0.5 mM PMSF, 0.5 mM AEBSF]. After elution (buffer A with 250 mM imidazole), the protein was finally purified by gel filtration over Superdex200 (GE Healthcare) in buffer B [10 mM Tris-HCl (pH 8.0), 0.7 M NaCl, 0.05% glycerol, 2 mM 2-mercaptoethanol], and concentrated to 14 mg/ml using a Millipore concentrator (Mol. wt. cutoff 10,000).

Mutants were created using the QuickChange system (Stratagene). All DNA constructs were verified by DNA sequencing.

Crystallization, data collection, and structure determination

Crystals of apo His_6-Cdc14p (residues 1-374, wild type) were grown at 20 °C from 14 mg/ml protein by hanging drop vapor diffusion against 0.1 M Bis-Tris (pH 6.0), 0.1 M ammonium sulfate, and 6% PEG4000. Crystals were cryoprotected using mother liquor containing 13% PEG4000 and 18% glycerol, and flash-cooled in liquid nitrogen. X-ray diffraction datasets were collected at 95 K at Photon Factory beamline BL-17A using an ADSC Quantum 270 CCD detector at a wavelength of 0.98 Å. Diffraction data were processed using iMOSFLM and CCP4 programs.[18,19] The structure was solved by

molecular replacement using MOLREP[20] using the structure of the catalytic domain of human Cdc14B (PDB code, 1OHE)[11] as a search model. The structure was refined by iterative cycles of model building using COOT[21] and refinement using PHENIX.[22] The final model geometry was validated by MolProbity.[23]

The Cdc14p-phosphopeptide complex was obtained by soaking method. S160-phosphorylated Swi6p peptide 155-HRELG-pS-PLKK-164 was synthesized by Sigma-Aldrich Japan. Crystals of apo His_6-Cdc14p (residues 1-374, C283S mutant) were grown at 20 °C from 14 mg/ml protein by hanging drop vapor diffusion against 0.1 M Bis-Tris (pH 6.0), 0.1 M ammonium sulfate, and 6% PEG4000. The Swi6p phosphopeptide was soaked into the apocrystals of C283S mutant in mother liquor supplemented with 11 mM peptide for 2 h. Crystals were cryoprotected using mother liquor containing 13% PEG4000 and 18% glycerol, and flash-cooled in liquid nitrogen. X-ray diffraction datasets were collected at 95 K at Photon Factory beamline BL-5A using an ADSC Quantum 315r CCD detector at a wavelength of 1.0 Å. Diffraction data were processed using iMOSFLM and CCP4 programs.[18,19] The structures were solved by molecular replacement using MOLREP[20] using the structure of wild-type apo Cdc14p as a search model. The structures were refined by iterative cycles of model building using COOT[21] and refinement using PHENIX.[22] The final model geometry was validated by MolProbity.[23] Structural figures were produced using CCP4MG[24] and PyMOL.[25]

ConSurf analysis of evolutionary conservation

The evolutionary conservation profile of Cdc14 was estimated using ConSurf.[17] A CSI-BLAST search for homologs of the budding yeast Cdc14p sequence was performed against the UNIREF90 database with an E-value cutoff of 0.00001, minimal % ID of 35% for homologs and maximal % ID of 95% between sequences. A total of 150

homologous sequences were retrieved and multiply aligned using MAFFT. Calculation of position-specific conservation scores was performed using the Bayesian method.

Analytical gel filtration chromatography

To analyze the oligomeric state of the catalytic domain of Cdc14p in solution, we gel-filtered His_6-Cdc14p (residues 1-374) in buffer C (10 mM Tris-HCl pH 7.5, 0.6 M NaCl, 2 mM β-mercaptoethanol) with a Superdex200 10/300 GL column (GE Healthcare) calibrated with globular proteins of known molecular weight. Each injection used 0.1 ml of 0.3 mg/ml His_6-Cdc14p (residues 1-374), and the elution from the column was monitored using the ultraviolet absorbance at 280 nm. The molecular mass of His_6-Cdc14p (residues 1-374) calculated from its amino acid sequence (including the N-terminal tag) is 48 kDa.

In vivo functional analysis

The *in vivo* function of Cdc14p mutants was assessed using a plasmid shuffle technique.[26] For the plasmid shuffle, plasmids (*CEN*, *LEU2*) encoding the wild type Cdc14p (full-length) or Cdc14p mutants (full-length) expressed from the *CDC14* promoter, or a control vector (pRS315)[27] were each transformed into haploid *cdc14Δ* yeast cells (*his3Δ1 leu2Δ0 ura3Δ0 cdc14Δ::kanMX4*) containing a wild-type *CDC14* maintenance plasmid (*CEN*, *URA3*). Single transformants were grown in SC-Ura-Leu medium at 30 °C for 1 day to saturation, diluted to an OD_{600} of 0.3, and grown in SC-Ura-Leu medium at 30 °C for 4 h to an OD_{600} of 1.2. Yeast cells were then serially diluted 1:6, and spotted onto 5-fluoroorotic acid (5-FOA) plates. 5-FOA eliminates the *URA3* maintenance plasmid encoding wild-type Cdc14p. Plates were incubated at 30 °C or 37 °C for 3 days.

Accession numbers

The atomic coordinates and structure factors have been deposited in the PDB with accession codes 5XW4 [apo Cdc14p (wild type)] and 5XW5 [Cdc14p (C283S) bound to the Swi6p phosphopeptide].

Supplementary Material

Additional Supporting Information may be found in the online version of this article.

Acknowledgments

We thank Hidemi Hirano for technical assistance and discussion. We also thank the staff of Photon Factory for assistance during X-ray diffraction data collection.

Conflict of Interest Statement

The authors have no conflict of interest to declare.

References

1. Wurzenberger C, Gerlich DW (2011) Phosphatases: providing safe passage through mitotic exit. Nat Rev Mol Cell Biol 12:469-482.
2. Stegmeier F, Amon A (2004) Closing mitosis: the functions of the Cdc14 phosphatase and its regulation. Ann Rev Genet 38:203-232.
3. Shou W, Seol JH, Shevchenko A, Baskerville C, Moazed D, Chen ZW, Jang J, Shevchenko A, Charbonneau H, Deshaies RJ (1999) Exit from mitosis is triggered by Tem1-dependent release of the protein phosphatase Cdc14 from nucleolar RENT complex. Cell 97:233-244.
4. Visintin R, Hwang ES, Amon A (1999) Cfi1 prevents premature exit from mitosis by anchoring Cdc14 phosphatase in the nucleolus. Nature 398:818-823.
5. D'Amours D, Stegmeier F, Amon A (2004) Cdc14 and condensin control the dissolution of cohesin-independent chromosome linkages at repeated DNA. Cell 117:455-469.
6. Sullivan M, Higuchi T, Katis VL, Uhlmann F (2004) Cdc14 phosphatase induces rDNA condensation and resolves cohesin-independent cohesion during budding yeast anaphase. Cell 117:471-482.
7. Clemente-Blanco A, Mayan-Santos M, Schneider DA, Machin F, Jarmuz A, Tschochner H, Aragon L (2009) Cdc14 inhibits transcription by RNA polymerase I during anaphase. Nature 458:219-222.
8. Wan J, Xu H, Grunstein M (1992) CDC14 of Saccharomyces cerevisiae. Cloning, sequence analysis, and transcription during the cell cycle. J Biol Chem 267:11274-11280.
9. Taylor GS, Liu Y, Baskerville C, Charbonneau H (1997) The activity of Cdc14p, an oligomeric dual specificity protein phosphatase from Saccharomyces cerevisiae, is required for cell cycle progression. J Biol Chem 272:24054-24063.
10. Mocciaro A, Schiebel E (2010) Cdc14: a highly conserved family of phosphatases with non-conserved functions? J Cell Sci 123:2867-2876.
11. Gray CH, Good VM, Tonks NK, Barford D (2003) The structure of the cell cycle protein Cdc14 reveals a proline-directed protein phosphatase. EMBO J 22:3524-3535.

12. Geymonat M, Spanos A, Wells GP, Smerdon SJ, Sedgwick SG (2004) Clb6/Cdc28 and Cdc14 regulate phosphorylation status and cellular localization of Swi6. Mol Cell Biol 24:2277-2285.
13. Kabsch W, Sander C (1983) Dictionary of protein secondary structure: pattern recognition of hydrogen-bonded and geometrical features. Biopolymers 22:2577-2637.
14. Wang WQ, Bembenek J, Gee KR, Yu H, Charbonneau H, Zhang ZY (2004) Kinetic and mechanistic studies of a cell cycle protein phosphatase Cdc14. J Biol Chem 279:30459-30468.
15. Barford D, Das AK, Egloff MP (1998) The structure and mechanism of protein phosphatases: insights into catalysis and regulation. Ann Rev Biophys Biomol Struct 27:133-164.
16. Carugo O, Argos P (1997) Protein-protein crystal-packing contacts. Protein Sci 6:2261-2263.
17. Ashkenazy H, Erez E, Martz E, Pupko T, Ben-Tal N (2010) ConSurf 2010: calculating evolutionary conservation in sequence and structure of proteins and nucleic acids. Nucleic Acids Res 38:W529-533.
18. Collaborative Computational Project, Number 4 (1994) The CCP4 suite: programs for protein crystallography. Acta Crystallogr D Biol Crystallogr 50:760-763.
19. Winn MD, Ballard CC, Cowtan KD, Dodson EJ, Emsley P, Evans PR, Keegan RM, Krissinel EB, Leslie AG, McCoy A, McNicholas SJ, Murshudov GN, Pannu NS, Potterton EA, Powell HR, Read RJ, Vagin A, Wilson KS (2011) Overview of the CCP4 suite and current developments. Acta Crystallogr D Biol Crystallogr 67:235-242.
20. Vagin A, Teplyakov A (1997) MOLREP: an automated program for molecular replacement. J Appl Cryst 30:1022-1025.
21. Emsley P, Lohkamp B, Scott WG, Cowtan K (2010) Features and development of Coot. Acta Crystallogr D Biol Crystallogr 66:486-501.
22. Adams PD, Afonine PV, Bunkoczi G, Chen VB, Davis IW, Echols N, Headd JJ, Hung LW, Kapral GJ, Grosse-Kunstleve RW, McCoy AJ, Moriarty NW, Oeffner R, Read RJ, Richardson DC, Richardson JS, Terwilliger TC, Zwart PH (2010) PHENIX: a comprehensive Python-based system for macromolecular structure solution. Acta Crystallogr D Biol Crystallogr 66:213-221.

23. Chen VB, Arendall WB, 3rd, Headd JJ, Keedy DA, Immormino RM, Kapral GJ, Murray LW, Richardson JS, Richardson DC (2010) MolProbity: all-atom structure validation for macromolecular crystallography. Acta Crystallogr D Biol Crystallogr 66:12-21.
24. McNicholas S, Potterton E, Wilson KS, Noble ME (2011) Presenting your structures: the CCP4mg molecular-graphics software. Acta Crystallogr D Biol Crystallogr 67:386-394.
25. The PyMOL Molecular Graphics System, Version 1.8, Schrödinger, LLC.
26. Boeke JD, Trueheart J, Natsoulis G, Fink GR (1987) 5-Fluoroorotic acid as a selective agent in yeast molecular genetics. Methods Enzymol 154:164-175.
27. Sikorski RS, Hieter P (1989) A system of shuttle vectors and yeast host strains designed for efficient manipulation of DNA in Saccharomyces cerevisiae. Genetics 122:19-27.

Figure legends

Figure 1. Structure of the catalytic domain of budding yeast Cdc14p. (A) The electron density of the Swi6p phosphopeptide bound to Cdc14p. The omit F_o–F_c map covering the Swi6p phosphopeptide is shown in blue mesh (contoured at 3.0σ) with the refined model of the Swi6p phosphopeptide. (B) Superposition of budding yeast Cdc14p (green) and human Cdc14B (orange; PDB code, 1OHE). (C) Two orthogonal views showing the overall structure of the catalytic domain of budding yeast Cdc14p (C283S; ribbon representation) bound to the Swi6p phosphopeptide (stick representation). The A- and B-domains are colored blue and green, respectively. The linker helix connecting the A- and B-domains is colored purple. The C-terminal extension is colored orange. (D) Primary structure of the catalytic domain of Cdc14p, with secondary structure assignment. (E) A stereo view of the interactions between Cdc14p (ribbon representation) and the Swi6p phosphopeptide (stick representation with yellow carbons) at the substrate-binding cleft formed at the interface of the A-domain (blue) and the B-domain (green). The Cdc14p residues that are involved in the recognition of the phosphopeptide substrate are shown in stick representation with orange carbons. Dashed lines represent hydrogen bonds or salt bridges.

Figure 2. Dimerization of Cdc14p. (A) Two orthogonal views showing the ribbon diagram of Cdc14p homodimer in the asymmetric unit. The two Cdc14p chains are distinguished by the colors dark green and orange. The dimer interface residues are shown in stick representation. The Swi6p phosphopeptide (stick representation) is bound to the catalytic site of Cdc14p chain A (green), whereas a sulfate ion (stick representation) is bound to the catalytic site of Cdc14p chain B (orange). Dashed lines represent hydrogen bonds. (B) The backside of the Cdc14p catalytic site. The dimer interface residues are shown in stick representation, together with ribbon diagram of

Cdc14p chain A and stick representation of Swi6p. Chain B of Cdc14p is not shown for clarity. (C) Gel filtration analysis of the catalytic domain of wild type and mutant Cdc14p. (D) Standard curve for estimation of molecular masses (M_r) of Cdc14p oligomers. $K_{av} = (V_e - V_o)/(V_t - V_o)$, where V_e = elution volume, V_o = void volume, and V_t = total volume. (E) Functional analysis of Cdc14p in yeast. Complementation of *cdc14Δ* by vector alone, wild type *CDC14*, and mutant *CDC14* alleles containing the mutation(s) at the dimerization interface.

Table I. *Crystallographic Statistics*

Crystal	apo Cdc14p (wild-type)	Cdc14p (C283S) bound to the Swi6p phosphopeptide
Data collection		
Space group	$P2_12_12_1$	$P2_12_12_1$
Unit cell dimensions		
a, *b*, *c* (Å)	82.85, 95.13, 137.76	82.93, 95.93, 136.62
α, β, γ (degree)	90, 90, 90	90, 90, 90
Wavelength (Å)	0.98	1.0
X-ray source	BL-17A, PF	BL-5A, PF
Resolution range (Å)[a]	55.79-1.85 (1.88-1.85)	30.59-1.85 (1.88-1.85)
No. of measured reflections[a]	611776 (15667)	355151 (10066)
No. of unique reflections[a]	91638 (3747)	91878 (3652)
Completeness (%)[a]	98.1 (82.2)	97.0 (79.2)
R_{merge} (%)[a]	6.3 (61.6)	5.9 (44.2)
Mean $I/\sigma(I)$[a]	16.5 (1.7)	13.8 (2.3)
Mean *I* half-set correlation CC(1/2)[a]	0.999 (0.744)	0.999 (0.809)
Multiplicity[a]	6.7 (4.2)	3.9 (2.9)
Wilson *B* factor (Å^2)	22.3	19.7
Refinement		
Resolution range (Å)[a]	55.79-1.85 (1.87-1.85)	30.59-1.85 (1.87-1.85)
R_{work} (%)[a]	17.8 (27.3)	19.1 (24.8)
R_{free} (%)[a]	20.3 (32.7)	21.7 (30.7)
No. of atoms		
Cdc14p	5955	5857
Swi6p	-	60
Sulfate	0	5
Water	571	666
No. of amino acids	737	734
Mean *B* factor (Å^2)		
Cdc14p	31.7	26.9
Swi6p	-	28.7
Sulfate	-	19.7
Water	38.1	34.8
RMSD from ideality		
Bond lengths (Å)	0.004	0.006
Bond angles (degree)	0.665	0.758
Protein geometry[b]		
Rotamer outliers (%)	0.16	0
Ramachandran favored (%)	96.02	96.94
Ramachandran outliers (%)	0.27	0.28
Cβ deviations > 0.25 Å (%)	0	0
MolProbity score (percentile)	1.29 (98)	1.29 (99)
PDB code	5XW4	5XW5

[a] Values in parentheses are for the highest-resolution shell.

[b] MolProbity was used to analyze the structures.

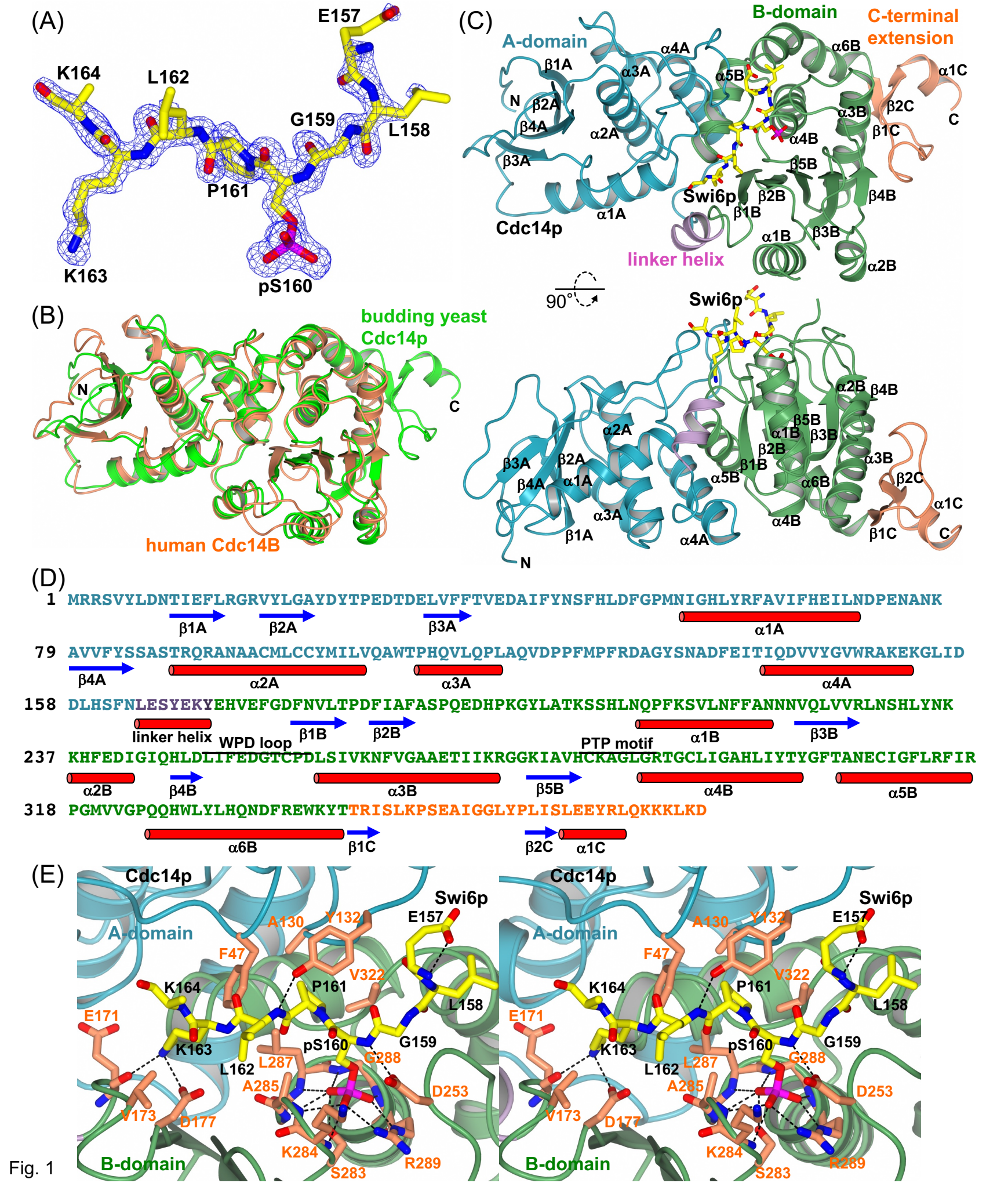
(A)
E157
K164
L162
G159
L158
P161
K163
pS160
(B)
budding yeast
Cdc14p
N
C
human Cdc14B
(C)
B-domain
C-terminal
extension
A-domain
α4A
α6B
β1A
α3A
α5B
α1C
N
β2A
β4A
α2A
α3B
β2C
C
β1C
α4B
β3A
β5B
Swi6p
β2B
β4B
α1A
β1B
Cdc14p
α1B
β3B
linker helix
α2B
90°
Swi6p
α2B
β4B
β5B
α2A
α1B
β3B
β2B
β3A
β2A
α3B
β1B
β4A
α1A
α5B
α6B
β2C
α1C
α3A
α4B
β1A
α4A
β1C
C
N
(D)
1 MRRSVYLDNTIEFLRGRVYLGAYDYTPEDTDELVFFTVEDAIFYNSFHLDFGPMNIGHLYRFAVIFHEILNDPENANK
β1A
β2A
β3A
α1A
79 AVVFYSSASTRQRANAACMLCCYMILVQAWTPHQVLQPLAQVDPPFMPFRDAGYSNADFEITIQDVVYGVWRAKEKGLID
β4A
α2A
α3A
α4A
158 DLHSFNLESYEKYEHVEFGDFNVLTPDFIAFASPQEDHPKGYLATKSSHLNQPFKSVLNFFANNNVQLVVRLNSHLYNK
linker helix
β1B
β2B
α1B
β3B
237 KHFEDIGIQHLDLIFEDGTCPDLSIVKNFVGAAETIIKRGGKIAVHCKAGLGRTGCLIGAHLIYTYGFTANECIGFLRFIR
WPD loop
PTP motif
α2B
β4B
α3B
β5B
α4B
α5B
318 PGMVVGPQQHWLYLHQNDFREWKYTTRISLKPSEAIGGLYPLISLEEYRLQKKKLKD
α6B
β1C
β2C
α1C
(E)
Cdc14p
Swi6p
A-domain
A130
Y132
E157
F47
V322
K164
P161
L158
E171
K163
pS160
G159
L162
L287
G288
A285
D253
V173
D177
K284
B-domain
S283
R289
Cdc14p
Swi6p
A-domain
A130
Y132
E157
F47
V322
K164
P161
L158
E171
K163
pS160
G159
L162
L287
G288
A285
D253
V173
D177
K284
B-domain
S283
R289

Fig. 1

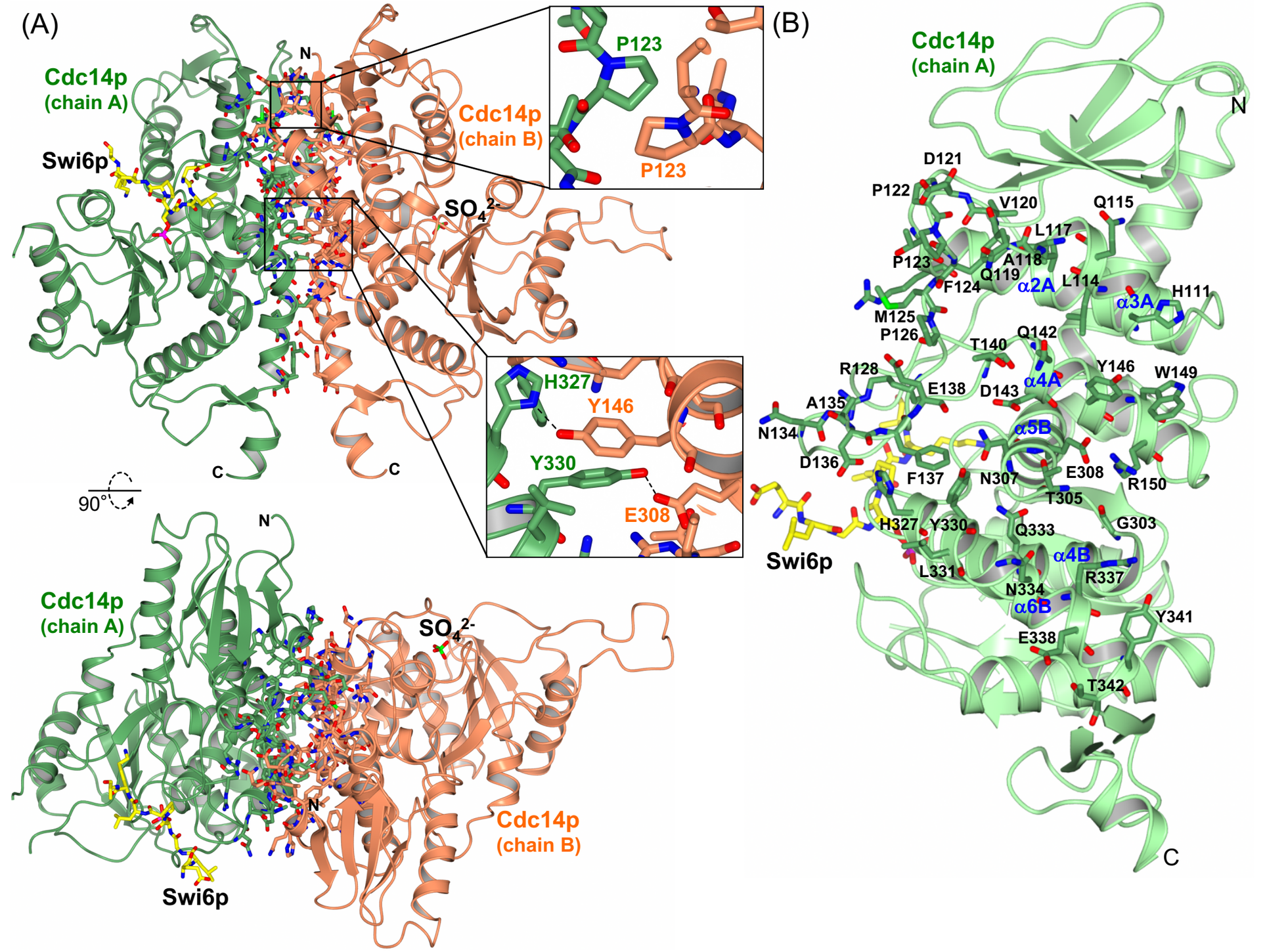
(A)
Cdc14p
(chain A)
Swi6p
N
Cdc14p
(chain B)
P123
P123
SO_4^{2-}
H327
Y146
Y330
E308
C
C
90°
N
Cdc14p
(chain A)
SO_4^{2-}
N
Cdc14p
(chain B)
Swi6p
(B)
Cdc14p
(chain A)
N
D121
P122
V120
Q115
L117
P123
A118
Q119
F124
α2A
L114
H111
α3A
M125
P126
Q142
T140
R128
Y146
W149
E138
D143
α4A
A135
N134
α5B
D136
F137
N307
E308
R150
T305
H327
Y330
Q333
G303
Swi6p
α4B
L331
R337
N334
α6B
Y341
E338
T342
C
(C)
wild type
P123E
Y146K/Y330K
A_{280}
Elution volume (ml)
(D)
RNase A (13 kDa)
Carbonic anhydrase
(29 kDa)
mutants
(33 kDa)
Ovalbumin (43 kDa)
wild type
(76 kDa)
BSA (66 kDa)
Catalase (232 kDa)
Ferritin, type 1 (440 kDa)
K_{av}
Log M_r
(E)
30℃
37℃
vector
wild type
P123E
Y146K/Y330K

Fig. 2

SUPPORTING INFORMATION

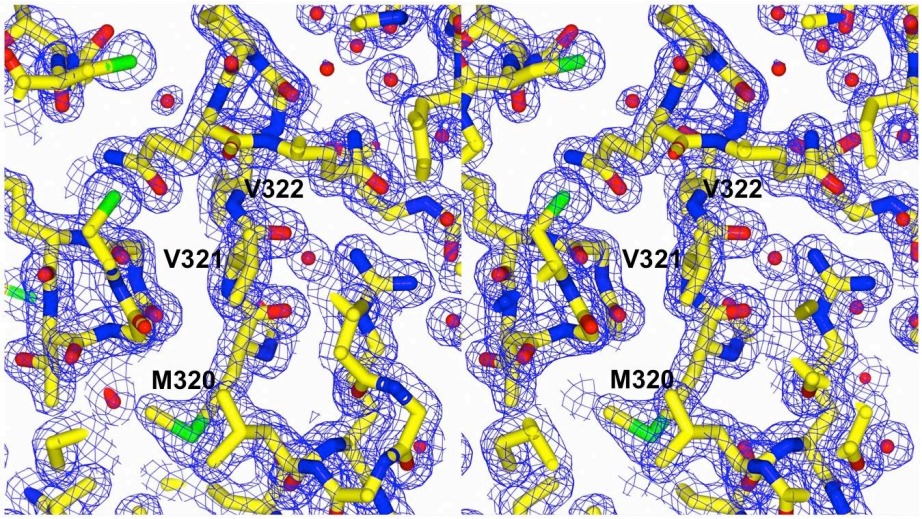

Figure S1. Stereoview of a piece of $2F_O–F_C$ electron density map of the wild-type apo crystal of Cdc14p. The map was contoured at 1.5σ and corresponds to the electron densities at and around V321.

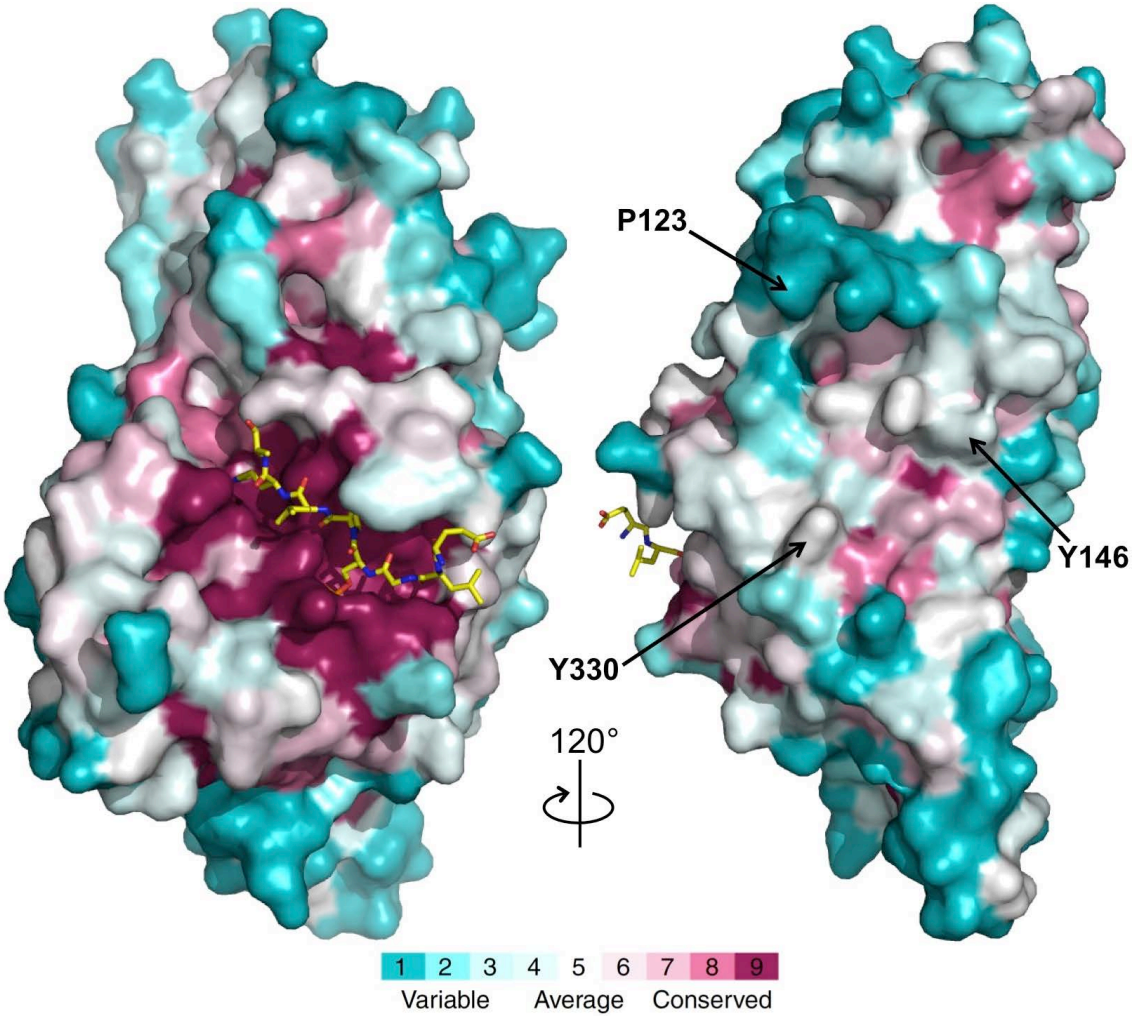

Figure S2. Cdc14p surface colored according to sequence conservation, from the most conserved (dark magenta) to the most divergent (dark cyan), using the ConSurf web server (htttp://consurf.tau.ac.il/). S160-phosphorylated Swi6p peptide bound to the catalytic site of Cdc14p is shown in stick representation. The figure on the right-hand side is shown in the same orientation as in Figure 2(B).